

Short Paper

Iris Recognition Using Gabor Filters and the Fractal Dimension

C. C. TSAI, J. S. TAUR AND C. W. TAO*

*Department of Electrical Engineering
National Chung Hsing University
Taichung, 402 Taiwan*

**Department of Electrical Engineering
National I-Lan University
I-Lan, 260 Taiwan*

Iris recognition is an emerging noninvasive biometric technology. The iris is very suitable for the verification and the identification of humans due to its distinctive and stable spatial patterns. In this paper, we propose an effective iris recognition algorithm which adopts a bank of Gabor filters combined with the estimated fractal dimension. After the preprocessing procedure, the normalized effective iris region is decomposed according to different frequency regions by the multi-channel Gabor filters. The texture information of the filtered images is obtained via the differential box-counting method. A feature selection scheme is then adopted to remove the unimportant features to reduce the amount of data and improve the performance. The experimental results on the CASIA database show that the proposed method has a very high recognition rate.

Keywords: biometrics, iris recognition, Gabor filters, fractal dimension, feature selection

1. INTRODUCTION

Biometric technologies for personal identification have been motivated by the growing need of security in recent years. The traditional security systems based on passwords, ID cards, or other equipments may be inconvenient or cracked. In contrast, biometric techniques utilize physiological or behavioral characteristics, such as the face, fingerprint, palm print, iris, retina, voice and gait, *etc.*, to accurately authenticate human's identity. These techniques exhibit the advantages of reliability and convenience.

The human iris is a ring between the pupil and the sclera. It has distinctive spatial patterns with the properties of being unique to each people and stable with age. After teenage, the healthy iris will remain almost unchanged [1]. Similar to the face and the fingerprints, the iris appears outside. However, the iris is behind the cornea and is therefore difficult to be faked or fabricated. From this point of view, iris recognition has more advantages over other biometric identification technologies.

For the last decade, iris recognition has been a popular research topic of biometrics. A typical and successful iris recognition system was developed by Daugman [2]. Daugman's system used the first order derivatives of image intensity to locate the circular edges of the iris, and made use of multiscale quadrature 2-D Gabor wavelets to capture

Received May 14, 2007; revised October 14, 2007; accepted November 12, 2007.
Communicated by Pau-Choo Chung.

the information of the local phase. The feature vector was generated by quantizing the local phase angle according to the outputs of the real and imaginary part of the filtered images. Wildes *et al.* [3] used a Laplacian pyramid constructed with four different resolution levels to extract the iris feature. Boles and Boashash [4] adopted the zero-crossing representation of a 1-D dyadic wavelet transform at different resolution levels to represent the feature of the iris. Zhu, Tan and Wang [5] adopted the multi-channel Gabor filters with six frequencies and four orientation bands to decompose the iris image. The feature vector of the iris pattern was composed of the mean and the standard deviation of each output image. Texture analysis-based method [6] and the local intensity variation analysis-based methods [7, 8] were proposed by Ma, Tan, Wang, and Zhang to extract the feature of the iris image. Noh *et al.* [9] made use of the independent component analysis (ICA) to generate optimal basis functions to represent the one dimensional iris signals. The coefficients of the ICA expansions were then used as the features. H. Proença *et al.* [10] divided the iris image into six regions and extracted the feature of each region independently. They then developed a classification rule to fuse the dissimilarity value of each region.

The feature extraction method based on the fractal dimension was first proposed to estimate length of coastline [11]. Several algorithms have been proposed to estimate the fractal dimension of a 2-D image such as [12-15]. The fractal dimension can be used to analyze the texture of iris images effectively [16, 17] and it has not been adopted to describe the Gabor filtered [18] images in the previous iris recognition system. In our experiments, we find that the Gabor decomposed images can provide adequate texture information for different frequency bands which can be effectively represented by the fractal dimension to offer a good performance. Furthermore, in the previous iris recognition systems, the whole adopted iris area is treated equally. However, the importance of the iris features from different locations and different channels of the Gabor decomposition may be different. Accordingly, we use a feature selection method to remove the unimportant features. In our experiments, the proposed scheme could improve the system performance substantially.

There are three major steps in the proposed recognition system: the image preprocessing, the feature extraction, and the feature matching. The framework of our system is illustrated in Fig. 1. This paper is organized as follows. Section 2 describes the preprocessing method for iris images, which includes the iris localization, the image normalization,

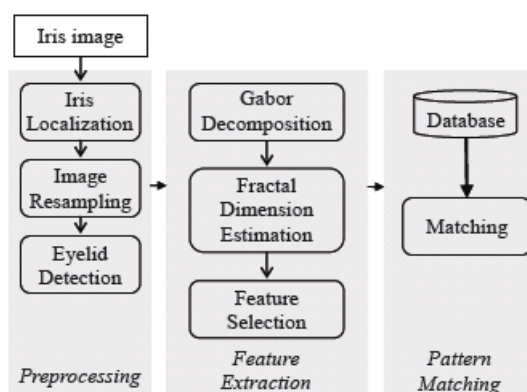


Fig. 1. Block diagram of the proposed iris recognition system.

and the lower eyelid detection. Section 3 presents the feature extraction, feature selection, and the feature matching scheme for the iris images. Experimental results are reported in section 4. Finally, section 5 concludes this paper.

2. IRIS IMAGE PREPROCESSING

The image around the eye contains the iris, the pupil, the sclera, and some eye surroundings (*e.g.*, Eyelashes, eyelids, *etc.*) The variation of the pupillary dilation and different camera-to-eye distances could result in varied sizes of iris images. In the preprocessing step, the iris region is located from the original image of the eye, and then normalized to a fixed size.

2.1 Iris Localization

The location of the iris is between the pupil and the sclera. We model the boundaries of the limbus and the pupil with circular contours. It is assumed that these two circles are not necessarily concentric. In the database we use [19], the pupil is typically darker than the other part of the eye. Therefore, we project the iris image in the vertical and horizontal directions. Then the rough coordinate of the center of the pupil can be obtained by calculating the positions of the minima of the projections. The accurate parameters of the pupil and limbus are obtained by using the Canny operator [20] and the Hough transform [21] near the rough center of the pupil. This two-step localization method can reduce the searching time of the Hough transform. A typical result of iris localization is shown in Fig. 2 (a) where the centers of the limbus and the pupil are marked with a red circle and a blue cross, respectively.

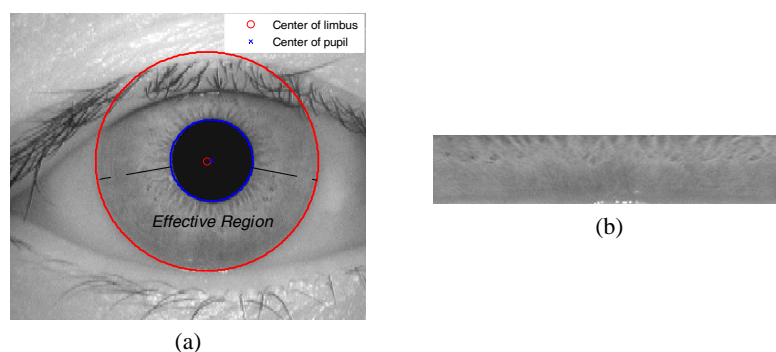


Fig. 2. (a) Inner and outer boundaries of the iris image; (b) Normalized iris block image of (a).

2.2 Resampling

In general, the size of an iris may vary due to different eyes, camera-to-eye distances, and the degrees of the pupil dilation. Such deformation will decrease the correct matching rate. Also, the upper portion of the iris is usually partly occluded by the eyelid and/or eyelashes. The occluded iris image may cause incorrect matching.

In order to obtain a higher recognition rate, it is necessary to compensate or eliminate such deformation and noise. In our system, we discard the upper portion of the iris and unwrap the pre-selected part of iris image (between 191° and 350° , cf. Fig. 2 (a)) to a rectangular block of the fixed size 64×320 pixels by using the bicubic interpolation. An example of the resampled iris is shown in Fig. 2 (b).

2.3 Eyelid Detection

As shown in Fig. 3 (a), the lower portion of the resampled iris block is sometimes occluded by the lower eyelid and/or eyelashes. The area of the occlusion can vary a lot if the human operator is not constrained. The occlusion of the lower eyelid will seriously destroy the information of the iris texture and affect the matching rate. Such useless portion must be detected and masked out. The eyelid detection is performed by using the Canny edge detector and the curve fitting of a second-order polynomial. The ratio of the masked area to the area of the entire iris block can be used to assess the information sufficiency of the iris block. In our experiments, the recognition accuracy can be improved by rejecting the samples with a large occluded area.

The iris image from the same eye may have different brightness due to the different conditions of image acquisition. In order to improve the recognition performance, the resampled iris block is normalized to have zero mean and unit variance after the removal of the eyelid. The results of the eyelid detection and the iris normalization are shown in Figs. 3 (b) and (c), respectively.

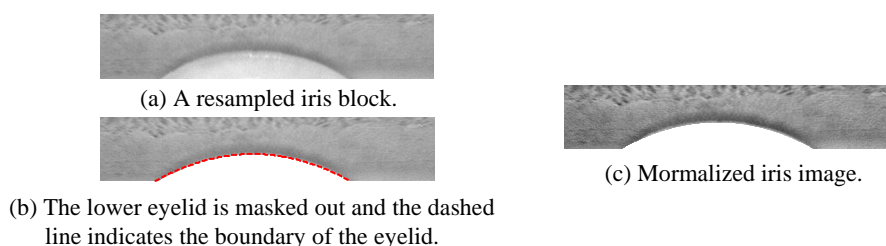


Fig. 3. Eyelid detection and image enhancement.

3. FEATURE EXTRACTION AND MATCHING

With the normalized iris image from the preprocessing step, proper iris features can be extracted. Then the recognition system can decide if the input iris pattern matches any iris in the database. In this paper, we utilize the Gabor filtering, the fractal dimension estimation [22], and the feature selection to extract the important features of the iris texture. The nearest-neighbor rule is then adopted to classify the feature vector.

3.1 Gabor Filter

According to [23], the multiresolution Gabor filters are similar to the 2-D receptive field profiles of the mammalian cortical simple cells. The Gabor decomposition adopts directional band-pass filters which have orientation-selective and frequency-selective pro-

erties. In our recognition system, we use the model of Gabor filters proposed in [24] where the impulse response of the j th frequency (ω_{r_j}) and the k th orientation (θ_k) band is defined as

$$G_{jk}(x, y) = \exp \left[-\frac{1}{2} (\sigma_{r_j}^2 (x \cos \theta_k + y \sin \theta_k)^2 + \sigma_{\theta_k}^2 (-x \sin \theta_k + y \cos \theta_k)^2) \right] \cdot \exp [2\pi i \omega_{r_j} (x \cos \theta_k + y \sin \theta_k)] \quad (1)$$

where $1 \leq j \leq m$ and $1 \leq k \leq n$. The angular bandwidth is chosen to be π/n , which results in

$$\sigma_{\theta_k} = \sigma_{\theta} = \frac{\pi}{2n}. \quad (2)$$

By choosing $0 < \omega_{r_{\min}} < \omega_{r_{\max}} < 1/2$, the radial centers and bandwidths can be obtained as follows:

$$\begin{aligned} \omega_{r_j} &= \omega_{r_{\min}} + \sigma_0 (1 + 3(2^{j-1} - 1)) \\ \sigma_{r_j} &= \sigma_0 \cdot 2^{j-1} \end{aligned} \quad (3)$$

$$\text{where } \sigma_0 = \frac{\omega_{r_{\max}} - \omega_{r_{\min}}}{2(2^m - 1)}. \quad (4)$$

In this situation, the normalized iris image can be decomposed into $m \times n$ component images by filtering the normalized iris image with the filters described above.

3.2 Fractal Dimension

In our recognition system, the iris component images are partitioned into blocks. Then the differential box-counting (DBC) method [14, 25] is adopted to estimate the fractal dimension of the blocks in the iris component images.

In the situation of an ideal fractal image, the fractal dimension (FD) can be computed using

$$FD = \frac{\log(N(r))}{\log(1/r)} \quad (5)$$

where r and $N(r)$ will be explained in the following. Since most of the texture images are not ideal fractal images, the fractal dimension is estimated as the slope of the least squares linear fit of $\log(N(r))$ against $\log(1/r)$ for general texture images in the DBC method. Let us consider an image block of size $M \times M$ pixels with a maximum gray-level G . Let r be defined as $r = s/M$ where s is an integer and $M/2 \geq s > 1$. Let the image be considered as a two-dimensional function $z(x, y)$ with the input (x, y) denoting the two-dimensional position and the third dimensional z denoting the gray-level of the image at that position. The three-dimensional space is partitioned into boxes of size $s \times s \times s$. The boxes are indexed with (i, j, k) in the (x, y, z) space. Assume that the minimum and maximum gray-levels of the image in the (i, j) th $s \times s$ image block on the (x, y) space fall

in the m th and the l th box in the z direction, respectively. Then the contribution to $N(r)$ in the (i, j) th $s \times s$ block can be computed as follow:

$$n_r(i, j) = l - m + 1. \quad (6)$$

Taking the contributions from all the blocks on the (x, y) space into consideration, we can obtain

$$N(r) = \sum_{i,j} n_r(i, j). \quad (7)$$

The $N(r)$ is computed for different values of r (*i.e.*, different sizes of the partitioned boxes.) Then the fractal dimension can be estimated as the slope of the least squares linear fit of $\log(N(r))$ against $\log(1/r)$.

3.3 Feature Vector

In our iris recognition system, the Gabor filters, the fractal dimension estimation, and a feature selection scheme are integrated to extract the effective representation of the distinctive spatial pattern in the iris image.

The normalized iris image is decomposed into 24 component images corresponding to three frequencies and eight orientation bands ($m = 3, n = 8$) by the Gabor decomposition. The size of each component image is 64×320 . Typical component images from a normalized iris image are shown in Fig. 4 (a). Each iris component image is partitioned into non-overlapping blocks of size 16×16 . Then the fractal dimension of each block is estimated. We can obtain 80 ($= 4 \times 20$) fractal dimension values for each component image as shown in Fig. 4 (b). Putting together all fractal dimensions from the image blocks of all component images, we can obtain the 1920-dimensional feature vector V for an iris image as

$$V = [FD_{1,1}, FD_{1,2}, \dots, FD_{1,80}, FD_{2,1}, \dots, FD_{24,79}, FD_{24,80}]^T \quad (8)$$

where T is the transpose operator. Each component of the feature vector is then uniformly quantized into eight-bit code.

3.3.1 Feature selection

In iris recognition, the generation of sufficient features should be based on the distinguishing characteristics of the images. The Gabor filters with a fixed number of decomposed bands may contain redundant features. In addition, the importance of the features from different locations of the iris may be different. As shown in Fig. 2, the region of the iris near the pupil usually exhibits more varied texture patterns when compared with the outer region. Therefore, a searching technique for a suitable subset of features is adopted to discard the features with the least discrimination and to select the features with more useful information. In this paper, the sequential forward floating search method (SFFS) [26] is adopted to select the features and the equal error rate (EER) is adopted as

the separability criterion. In order to compute EER, the distributions of inter-class distance and intra-class distance of samples are estimated using histogram approach. Therefore, the distance between two feature vectors is defined in the following.

As mentioned previously, each component image of the Gabor filter is partitioned into non-overlapping blocks of size 16×16 and the fractal dimensions of the blocks are then estimated. The fractal dimension values in each component image are grouped to form iris ribbons. Each component image contains four horizontal iris ribbons and there are 20 fractal dimension values in each iris ribbon as shown in Fig. 4 (b). Then totally 96 ($= 4 \times 24$) iris ribbons can be obtained for each iris image. For a pair of iris images, I_1 and I_2 , let E^α denote the set of effective elements in the α th corresponding iris ribbon pair, i.e., E^α contains the features that are both available (not masked out in the eyelid removal procedure, cf. sections 2.3) for the corresponding ribbons. Furthermore, let the vector comprising the distances between the iris ribbons be denoted as $X = [x_1, x_2, \dots, x_{96}]^T$.

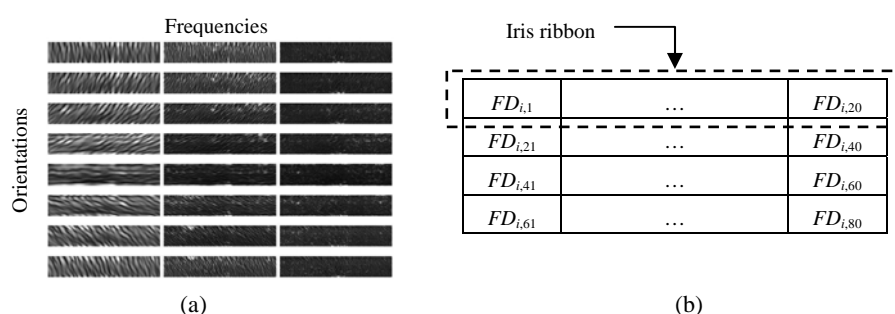


Fig. 4. (a) Shows the iris component images from Gabor filters, and (b) Indicates the corresponding fractal dimensions in the i th component image.

$$x_\alpha = \frac{1}{|E^\alpha|} \sum_{j=1, j \in E^\alpha}^{20} |U_1^{\alpha,j} - U_2^{\alpha,j}| \tag{9}$$

$$U_k^\alpha = \left[V_k^{(\alpha-1) \times 20 + 1}, \dots, V_k^{\alpha \times 20} \right]^T, \text{ for } \alpha = 1, 2, \dots, 96, k = 1, 2 \tag{10}$$

where $U_k^{\alpha,j}$ denotes the j th component of the α th iris ribbons of the pair of iris images I_k , V_k^γ represents the γ th element in the feature vector for image I_k in Eq. (8), and $|E^\alpha|$ is the number of elements in E^α . Note that the distance between the pair of iris images can be obtained from the distances between the iris ribbons by computing $\sum_{i=1}^n |E_i| x_i / \sum_{i=1}^n |E_i|$. The distributions of the distance for both the intra-class and the inter-class can be estimated by the corresponding histograms of the distances. Then, the false acceptance rate (FAR) and the false rejection rate (FRR) can be estimated for the different threshold values. The EER is the rate when the FAR is equal to the FRR for a specific threshold.

Let $Y_n = \{y_i: 1 \leq i \leq n, y_i \in X\}$ be the set of the best combination of the n distance features and $\bar{Y}_{96-n} \in X$ be the remaining distance features of X . Assume that the desired number of ribbons is N . The steps of the SFFS method are described in the following:

Step 1: Initialization: Let $n = 0$ and $Y_0 = \emptyset$.

1.1: Select an element of \bar{Y}_{96-n} which produces the lowest value of EER when it is combined with Y_n ; that is, $y^+ = \arg \min_{y \in \bar{Y}_{96-n}} EER(\{Y_n, y\})$; add this element into the best combination of the distance features ($Y_{n+1} = \{Y_n, y^+\}$), and let $n = n + 1$.

1.2: If $n < 2$, repeat step 1.a. (That is, the number of the features in the initial combination is two.)

Inclusion stage:

Step 2: Select an element of \bar{Y}_{96-n} which produces the lowest value of EER when it is combined with Y_n ; add this element into the best combination of the distance features ($Y_{n+1} = \{Y_n, y^+\}$), and let $n = n + 1$.

Test stage:

Step 3: Find the least significant element in Y_n ; that is, $y^- = \arg \min_{y \in Y_n} EER(Y_n - \{y\})$.

Step 4: If $y^- = y^+$ or $EER(Y_n - \{y^-\}) > EER(Y_{n-1})$,

4.1: If $n = N$, stop the algorithm; else go to step 2. (There is no need to perform the backward search, and the algorithm should be terminated or returned to the inclusion stage.)

Step 5: If $n = 3$ and $EER(Y_n - \{y^-\}) \leq EER(Y_{n-1})$, put $Y_{n-1} = Y_n - \{y^-\}$ and let $n = n - 1$; go to step 2.

Exclusion stage:

Step 6: Remove y^- from the best combination ($Y_{n-1} = Y_n - \{y^-\}$) and let $n = n - 1$. Clear y^+ and go to step 3. (Further backward search is required.)

The fractal dimension values of the blocks in the selected ribbons are collected to form a new feature vector V . In our experiment, this method can reduce the dimension of the iris feature vector and improve the system performance. The EERs for different numbers of features are discussed in section 4.4.

3.4 Matching

In the classification phase, the extracted feature vector V of the input iris image is compared with the feature vectors stored in the database to decide if V belongs to one of the persons in the database. The nearest-neighbor classifier is adopted in our algorithm. We assume that there are K iris classes in the database and there are L templates in each class. Let $V_{i,l}$ denote the l th template of the i th class in the database. The j th components of V and $V_{i,l}$ are denoted as V^j and $V_{i,l}^j$, respectively. Let $E_{i,l}$ denote the effective set of features for V and $V_{i,l}$, i.e., it contains the features of the common blocks of V and $V_{i,l}$ that are not masked out in the eyelid removal procedure. Only the blocks which are not masked out in either the template image or the test iris image are considered in the matching procedure. Therefore, the $L1$ distance measure can be defined as follows:

$$d_1(i, l) = \frac{1}{|E_{i,l}|} \sum_{j=1, j \in E_{i,l}}^{(N \times 20)} |V^j - V_{i,l}^j| \quad (11)$$

Where $|E_{i,l}|$ denotes the number of elements in $E_{i,l}$, and $(N \times 20)$ is the number of features. The input test iris image is assigned to class c which contains the template with the

smallest distance to V , *i.e.*, $c = \arg \min_{\substack{i \\ 1 \leq i \leq K \\ 1 \leq l \leq L}} d_1(i, l)$.

3.4.1 Alignment

To alleviate the undesired effects from the translation, scaling, and rotation of the iris images, the unknown iris image and template image must be aligned. Scaling results from the varied camera-to-eye distances and the pupil dilation. Translation and rotation are due to the positional and angular deviation of the human head about the optical axis of the camera, respectively.

The iris localization achieves the translation invariance. The resampling of the iris block image to a fixed size performs the normalization of the scale. The rotation of the original eye image corresponds to the translation of the normalized iris image. In the matching stage, the test iris image is rotated -4° , -2° , 0° , 2° , 4° by shifting the normalized image by -8 , -4 , 0 , 4 , 8 pixels in the horizontal direction. The invariance of rotation is achieved by selecting the minimum distance during the horizontal shifting.

4. EXPERIMENTAL RESULTS

In this section, we consider two application scenarios: classification and verification. First all the iris ribbons are used in the simulation. Then only the features obtained using the procedure described in section 3.3.1 are adopted. Simulations show that the performances are improved significantly in both classification and verification situations through the feature selection.

4.1 Iris Database

The proposed algorithm for iris recognition has been tested using the CASIA database [19] which contains 756 iris images with the resolution of 320×280 pixels. There are 108 iris classes with 7 different images in each iris class. The first three and remainder four iris images in each class are taken from different sessions.

4.2 Classification Results

In the classification (identification) mode, three images from each iris class are randomly chosen as the template images, and the remainder four images are used for testing. This procedure is repeated 35 times. The best accuracy of the DBC method is 100% and the average correct recognition rates (CRR) of the DBC approach is 99.89%.

In order to reduce the adverse effects of the occlusion of the lower eyelid, we designed an additional experimental condition for the classification mode. According to our eyelid detection method, the ratio of the occluded area to the re-sampled iris block can be computed. First, the iris samples with a ratio larger than the pre-selected threshold T_R are discarded. If the number of images remained in a class is less than four images, the class will be excluded from the database. Then three iris images are randomly chosen from each class as the templates, and the remaining images are used as the testing images. Finally, the amount of the false matching data is counted. For a specific occlusion threshold, the scheme is repeated one hundred times and the correct recognition rate

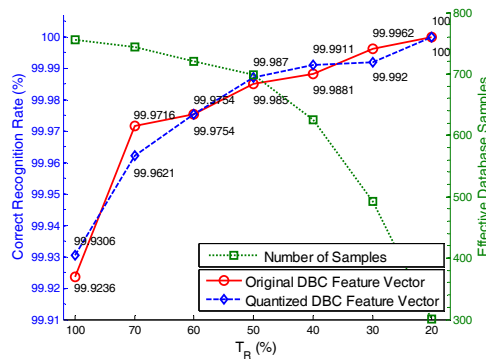


Fig. 5. The CRRs with the images rejected according to the occluded area. The horizontal axis indicates the threshold of the ratio of the masked-out area to the area of the entire iris block. When the threshold T_R becomes smaller, more iris images are rejected and the number of samples remaining in the data set is smaller as indicated with the green dotted line.

is computed. The experimental results are shown in Fig. 5. It is obvious that the recognition rate becomes higher as more iris images are rejected. Furthermore, the recognition rates with the original DBC features (without quantizing the elements into eight bits) are also plotted in Fig. 5. It can be observed that the quantized and the original feature vectors have very similar recognition performances.

4.3 Verification Results

In the verification experiments, the receiver operating characteristic (ROC) curve is used to evaluate the performance of our system. The FAR is the probability of accepting an imposter, and the FRR is the probability of rejecting a genuine user. For a given threshold T_v , the FAR is computed as the area under the inter-class distance distribution curve in the interval $[0, T_v]$. Similarly, the FRR is computed as the area under the intra-class distance distribution curve in the interval $[T_v, \infty]$. The EER is the error rate when the FAR is equal to the FRR at a specific threshold. The smaller EER indicates the better performance of a biometric verification system. In our experiments, the distances of the samples within the same class and between the different classes are computed using samples from different sessions. In each class, there are three samples from the first session and four samples from the second session, respectively. Therefore, totally 1296 ($= 3 \times 4 \times 108$) intra-class distances and 138672 ($= 3 \times 4 \times 107 \times 108$) inter-class distances are computed. The distributions of intra-class and inter-class distance of the proposed method are shown in Fig. 6, and the ROC curves are shown in Fig. 7. When all the iris ribbons are used, the EER of DBC is 0.72%.

Large iris area occluded by the eyelid may cause information insufficiency and result in lower matching rate. It is obvious in Fig. 7 that the EER is improved by rejecting iris images with large occlusion. The EER of DBC is reduced to 0.31%, when the iris images with the ratio of the occluded area is over 40% are rejected. Moreover, the performances using the quantized features are shown in Fig. 7 (b). Similar to the recognition case, the performances are about the same as those with original non-quantized features.

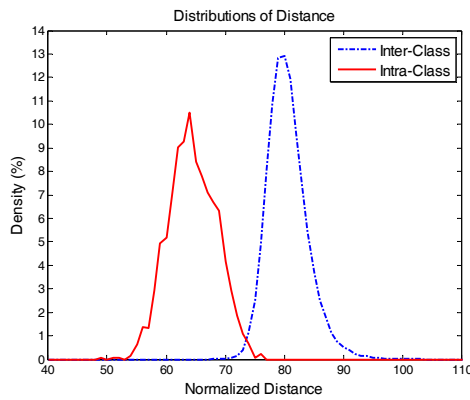


Fig. 6. The distance distributions for inter-class and intra-class patterns; the normalized distance is computed using Eq. (11).

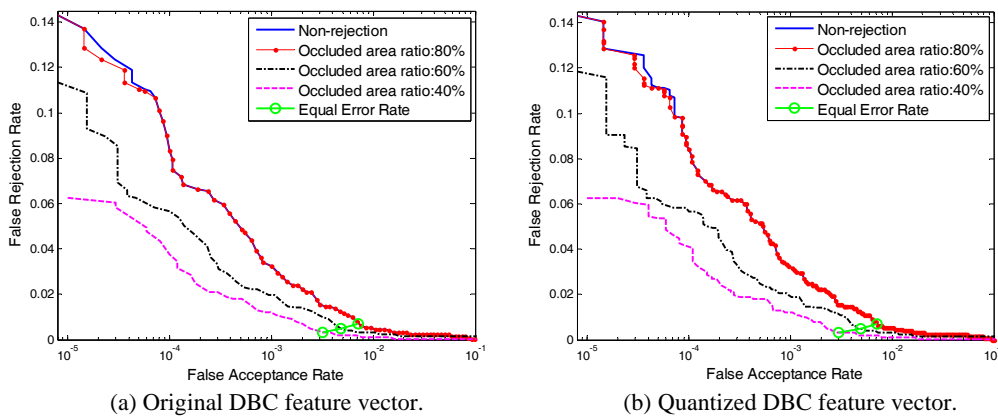


Fig. 7. The ROC curves and the equal error rates.

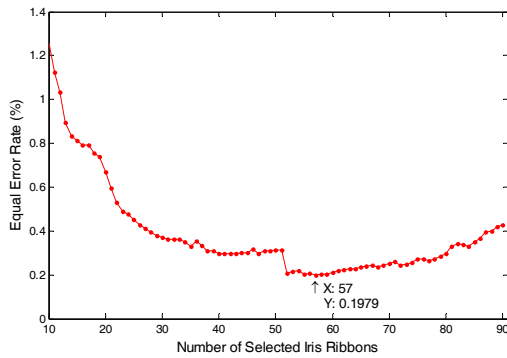


Fig. 8. The EERs for different number of ribbons obtained from the features selection algorithm with DBC method.

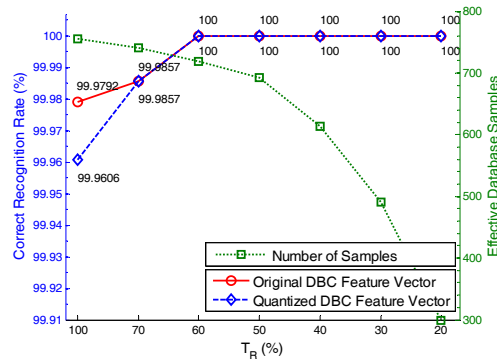


Fig. 9. The CRRs with the images rejected according to the occluded area with the best feature combinations. The horizontal axis indicates the threshold T_R of the ratio of the masked-out area to the area of the entire iris block.

4.4 Feature Selection

In order to eliminate the redundant features and select the iris ribbons with more discriminating power, we adopted a SFFS feature selection method based on minimizing the EER as described in section 3.3.1. The feature vectors of the searching method are formed by the distances of 96 iris ribbons. In the experiments, all iris samples are used to estimate the distance distributions. The EERs for different number of ribbons obtained from the features selection algorithm is shown in Fig. 8. The best EER (0.1979%) is achieved when 57 iris ribbons are selected. In other words, the dimension of the iris feature vector is 1140 ($= 20 \times 57$).

Two experiments described in section 4.2 are repeated using the best feature combination obtained previously to evaluate the identification performance. For the first method in section 4.2, the average CRR of the DBC method is increased to 99.9934%. (There is only one error in the experiment.) The results of the second experiments in section 4.2 are shown in Fig. 9. Compared with Fig. 5, the performances of the proposed method with both original and quantized feature vectors are improved. The CRR of DBC method with the selected features reaches to 100%, when the iris block images with the threshold T_R greater than sixty percent are rejected.

4.5 Discussions

Some major factors that will influence the performance of the iris recognition systems are discussed in the following. According to the experiments, we observe that a large difference in the area of the occlusion of the lower eyelid usually results in a large intra-class distance. This is also the main reason of the false matching in classification. Moreover, in iris localization procedure, we fit the edge of the pupil with a circular contour. However, the boundary of the pupil is not exactly a circle. This scheme may produce the inexact normalized iris image, and degrade the accuracy slightly. Another cause of large within-class distance is the varied positions of the light reflection. The violent noise of reflection will introduce a large intra-class distance, especially for the significantly varied area of occlusion of the lower eyelid. In order to reduce the effect of the reflection of the light, we are developing a noise detector that will detect the location of the reflection and discard the information around the location.

In practice, the relative differential box-counting (RDBC) method [13] is also implemented to evaluate the fractal dimension. In our experiment, the performance of Gabor filters combining with the DBC method substantially exceeds the RDBC method in both verification and classification modes.

Table 1. Comparison of verification results.

Methods	EER (%)	Method	EER (%)
SVMs [27]	2.63	DBC [29]	9.62
ICA [9]	0.34	Daugman [2]	0.29 [#] , 0.08 [*]
1-D fractal analysis [28]	4.63	Wildes [3]	1.76 [*]
EVWM [29]	3.85	Our proposed approach	0.20

^{**} and [#] indicate the experimental results of the re-implemented system in [8] and [9], respectively.

The performance comparison of several iris recognition systems is summarized in Table 1. Wang and Han [27] proposed an iris recognition algorithm using support vector machines. CASIA iris database was also used in this system. According to their experimental results, the EER of this scheme is 2.63% which is much larger than the best EER of our method (0.1979%). Noh *et al.*'s iris recognition system [9] adopted the independent component analysis method, and used the CASIA database to evaluate the system performance. The EER of Noh *et al.*'s system is 0.341% that is also worse than our method. Furthermore, Teo and Ewe [28] used the one-dimensional fractal analysis to extract the iris feature, and Wang *et al.* [29] proposed an extreme value weighted mean (EVWM) method to estimate the fractal dimension of the iris texture. Both the fractal dimension based systems used the CASIA database to validate the performance, and the EER of Teo's and Wang *et al.*'s algorithms are 4.63% and 3.85%, respectively. The DBC method is also implemented in [29] where the EER is 9.62%. Obviously, our system outperforms the basic fractal analysis based schemes due to the fact that the Gabor decomposition provides more information for the fractal estimation.

The well-known iris systems proposed by Daugman [2] and Wildes *et al.* [3] have been implemented by Ma *et al.* [8] to evaluate the performance of the existing iris systems with the CASIA database. According to their experiments, the EERs of Daugman system and Wildes system are 0.08% and 1.76%, respectively. However, the amount data of their database is different to the public CASIA database. The detailed experimental results of the existing iris recognition methods can be found in [8]. In addition, Noh *et al.* [9] also implemented the Daugman's method and used the public CASIA database to evaluate the EER which is equal to 0.29%.

5. CONCLUSIONS

In this paper, we proposed an iris recognition system based on the Gabor filters and the fractal dimension estimation. The sequential forward floating search method is adopted to select the iris ribbons with more discriminating power and to improve the system performance. The occlusion in the normalized iris image by the eyelid and eyelashes is detected and masked out in the matching procedure; hence the influence of occlusion on the matching rate is alleviated. By rejecting the iris image with large occlusion, the situation of insufficient information can be avoided, and the performance can be improved. The experimental results showed that our algorithm has a high performance in iris recognition application.

REFERENCES

1. F. H. Adler, *Physiology of the Eye*, St. Louis, MO, Mosby, 1965.
2. J. G. Daugman, "High confidence visual recognition of persons by a test of statistical independence," *IEEE Transactions on Pattern Analysis and Machine Intelligence*, Vol. 15, 1993, pp. 1148-1161.
3. R. P. Wildes, "Iris recognition: An emerging biometric technology," in *Proceedings of the IEEE*, Vol. 85, 1997, pp. 1348-1363.
4. W. W. Boles and B. Boashash, "A human identification technique using images of

- the iris and wavelet transform,” *IEEE Transactions on Signal Processing*, Vol. 46, 1998, pp. 1185-1188.
5. Y. Zhu, T. Tan, and Y. Wang, “Biometric personal identification based on iris patterns,” in *Proceedings of the 15th International Conference on Pattern Recognition*, Vol. 2, 2000, pp. 801-804.
 6. L. Ma, T. Tan, Y. Wang, and D. Zhang, “Personal identification based on iris texture analysis,” *IEEE Transactions on Pattern Analysis and Machine Intelligence*, Vol. 25, 2003, pp. 1515-1533.
 7. L. Ma, T. Tan, Y. Wang, and D. Zhang, “Local intensity variation analysis for iris recognition,” *Pattern Recognition*, Vol. 37, 2004, pp. 1287-1298.
 8. L. Ma, T. Tan, Y. Wang, and D. Zhang, “Efficient iris recognition by characterizing key local variations,” *IEEE Transactions on Image Processing*, Vol. 13, 2004, pp. 739-750.
 9. S. I. Noh, K. Bae, K. R. Park, and J. Kim, “A new iris recognition method using independent component analysis,” *IEICE Transactions on Information and Systems*, Vol. E88-D, 2005, pp. 2573-2581.
 10. H. Proença and L. A. Alexandre, “Toward non-cooperative Iris recognition: A classification approach using multiple signatures,” *IEEE Transactions on Pattern Analysis and Machine Intelligence*, Vol. 29, 2007, pp. 607-612.
 11. B. B. Mandelbrot, *Fractal Geometry of Nature*, Freeman, San Francisco, 1982.
 12. P. Asvestas, G. K. Matsopoulos, and K. S. Nikita, “Estimation of fractal dimension of images using a fixed mass approach,” *Pattern Recognition Letters*, Vol. 20, 1999, pp. 347-354.
 13. X. C. Jin, S. H. Ong, and Jayasooriah, “A practical method for estimating fractal dimension,” *Pattern Recognition Letters*, Vol. 16, 1995, pp. 457-464.
 14. N. Sarkar and B. B. Chaudhuri, “An efficient approach to estimate fractal dimension of textured images,” *Pattern Recognition*, Vol. 25, 1992, pp. 1035-1041.
 15. D. Talukdar and R. Acharya, “Estimation of fractal dimension using alternating sequential filters,” in *Proceedings of International Conference on Image Processing*, Vol. 1, 1995, pp. 231-234.
 16. W. S. Chen and S. Y. Yuan, “A novel personal biometric authentication technique using human iris based on fractal dimension features,” in *Proceedings of the International Conference on Acoustics, Speech and Signal Processing*, Vol. 3, 2003, pp. 201-204.
 17. P. S. Lee and H. T. Ewe, “Individual recognition based on human iris using fractal dimension approach,” *Lecture Notes in Computer Science*, Vol. 3072, 2004, pp. 467-474.
 18. B. J. Super and A. C. Bovik, “Localized measurement of image fractal dimension using Gabor filters,” *Journal of Visual Communication and Image Representation*, Vol. 2, 1991, pp. 114-128.
 19. CASIA, Iris Image Database version 1.0, <http://www.sinobiometrics.com>.
 20. J. Canny, “A computational approach to edge detection,” *IEEE Transactions on Pattern Analysis and Machine Intelligence*, Vol. 8, 1986, pp. 679-698.
 21. D. Ballard, “Generalized Hough transform to detect arbitrary patterns,” *IEEE Transactions on Pattern Analysis and Machine Intelligence*, Vol. 13, 1981, pp. 111-122.
 22. M. F. Barnsley, *Fractal Everywhere*, 2nd ed., Academic Press Professional, 1993.

23. J. Maikl and P. Perona, "Preattentive texture discrimination with early vision mechanisms," *Journal of Optical Society of America*, Vol. 7, 1990, pp. 923-932.
24. B. Duc, S. Fischer, and J. Bigün, "Face authentication with Gabor information on deformable graphs," *IEEE Transactions on Image Processing*, Vol. 8, 1999, pp. 504-516.
25. N. Sarkar and B. B. Chaudhuri, "An efficient differential box-counting approach to compute fractal dimension of image," *IEEE Transactions on Systems, Man and Cybernetics*, Vol. 24, 1994, pp. 115-120.
26. P. Pudil, J. Novovicova, and J. Kittler, "Floating search methods in feature selection," *Pattern Recognition Letters*, Vol. 15, 1994, pp. 1119-1125.
27. Y. Wang and J. Han, "Iris recognition using support vector machines," *Lecture Notes in Computer Science*, Vol. 3173, 2004, pp. 622-628.
28. C. C. Teo and H. T. Ewe, "An efficient one-dimensional fractal analysis for iris recognition," in *Proceedings of the 13th WSCG International Conference in Central Europe on Computer Graphics, Visualization and Computer Vision*, 2005, pp. 157-160.
29. C. Wang, S. Song, F. Sun, and L. Mei, "Iris recognition based on fractal dimension of extreme value weighted mean," in *Proceedings of the 6th World Congress on Intelligent Control and Automation*, Vol. 2, 2006, pp. 9949-9953.

C. C. Tsai (蔡仲智) received the B.S. and M.S. degrees in Electrical Engineering from National Chung Hsing University, Taiwan, R.O.C., in 2001 and 2003. He is currently a Ph.D. student in the Department of Electrical Engineering at National Chung-Hsing University, Taiwan, ROC. His research interests include neural networks, fuzzy logic system, and machine learning.

JinshiuH Taur (陶金旭) received his B.S. and M.S. degrees in Electrical Engineering from National Taiwan University, Taipei, Taiwan, R.O.C., in 1987 and 1989, and his Ph.D. degree in Electrical Engineering from Princeton University, in 1993. He was a Member of Technical Staff in Siemens Corporate Research, Inc. He is currently a Professor at the National Chung Hsing University in Taiwan. He received 1996 IEEE Signal Processing Society's Best Paper Award. His Primary research interests include neural networks, pattern recognition, computer vision, and fuzzy logic systems.

C. W. Tao (陶金旺) received the B.S. degree in Electrical Engineering from National Tsing Hua University, Hsinchu, Taiwan, R.O.C., in 1984, and the M.S. and Ph.D. degrees in Electrical Engineering from New Mexico State University, Las Cruces, in 1989 and 1992, respectively. He is currently a Professor with the Department of Electrical Engineering, National I-Lan University, I-Lan, Taiwan, R.O.C. He is an Associate Editor of the IEEE Transactions on Systems, Man, and Cybernetics. His research interests is on the fuzzy neural systems including fuzzy control systems and fuzzy neural image processing. Dr. Tao is an IEEE Senior Member and is listed in Who's Who in the world.